Analyst

Accepted Manuscript

Analyst

Analyst

ARTICLE TYPE

Highly-reproducible Raman scattering of NaYF$_4$:Yb,Er@SiO$_2$@Ag for methylamphetamine detection under near-infrared laser excitation

Yongmei Ma, Honglin Liu,* Zhenzhen Han, Liangbao Yang,* and Jinhuai Liu

This study reported the significantly improved Raman enhancement ability of silver nanoparticles (Ag NPs) by decorating themselves on single NaYF$_4$:Yb,Er@SiO$_2$ core-shell particles (UC@SiO$_2$@Ag) under a 785 nm excitation. The optimal thickness of silica shell can be easily obtained by adjusting the amounts of TEOS, which is the crucial element to balance the upconversion of UC and the formation of hot spot 10 by Ag NPs aggregation. This substrate revealed highly reproducible properties, which is crucial to practical application of SERS technology. This substrate exhibited an excellent sensitivity for methylamphetamine detection under near-infrared excitation. The advantages of NIR excitation in our SERS sensing open up a new application field of UC-noble metal composites, and also promise a new research direction for the synthesis and applications of SERS-active nanostructures.

15 Introduction

Surface-enhanced Raman scattering (SERS) technique has become one of the most widely pursued spectroscopic tools for the identification and detection of chemical and biological species and the molecular imaging and monitoring.[1-5] The spectroscopic 20 methods usually involve many factors, particularly, strongly relying on an external excitation light source.[6] The laser with low power levels may not produce the ideal sensitivity; to achieve a higher sensitivity as well as the improved temporal and spatial resolutions, a high laser power needs to be introduced. However, 25 high power levels may lead to a change in the structure of the target species, even damage the sample.[7] It is noted that the degree of SERS enhancement is strongly dependent on the excitation wavelength, with a sharp resonance Raman maximum for excitation at the wavelength of the Mie extinction maximum 30 of the metal particles.[8] The localized surface plasmon resonance (LSPR) occurs under conditions where the frequency of photons incident on the nanoparticles (NPs) is resonant with the collective excitation of its conduction electrons.[9] Excitation of the LSPR is characterized by wavelength-selective extinction and enhanced 35 electromagnetic fields at the NPs surface.[10, 11] Actually, LSPR frequencies of Ag and Au nanostructures locate in the UV/visible range, hence the excitation lasers used in most SERS studies were the UV/visible lights.[12-14] However, the laser power of UV/visible light may damage the target molecules for the long illumination 40 time, especially in the presence of O$_2$.[15] Moreover, the high laser power may result in a strong heating effect which may induce the photobleaching or desorption of the molecules in the probed volume and make the SERS signals undetectable.[16] Generally, the laser with longer wavelengths will have much deeper penetration 45 depth and relatively smaller damage to the sample, e.g. the near-infrared (NIR) lights which are not absorbed strongly by the

living tissues.[17] Nevertheless, for the purpose of obtaining the most excellent SERS performance, one has to tune the LSPR features of noble metal nanostructures to match the frequencies of 50 near-infrared lights.[18, 19] It is still an attractive challenge to develop the nanostructures that can well match the near-infrared excitation and generate high SERS enhancement under relatively lower levels of laser power.

Upconversion (UC) emission materials can convert infrared 55 radiation into visible light refers to non-linear optical processes that convert two or more low-energy pump photons to a higher-energy output photon. In addition, UC materials show a sharp emission bandwidth, large anti-Stokes shifts, high photostability, tunable emission, and low cytotoxicity, which leads to potential 60 applications in lasers, next-generation lighting, infrared quantum counters, biological macromolecular systems and has been used in a variety of assay formats ranging from bio-detection to cancer therapy.[20, 21] Recently, the coupling of UC nanocrystals with noble metal NPs such as Ag and Au has been developed as a 65 valuable strategy to enhance their luminescence.[22-24] So coupling the UC with noble metals is an attractive and promising strategy to solve the problem mentioned above. Our group have reported the significantly improved Raman enhancement and plasmon photocatalytic ability of Ag NPs by decorating themselves on 70 single NaYF$_4$:Yb,Er upconversion microcrystals (UC@Ag) under a 785 nm excitation with a relatively low laser power for the first time.[25] However, the excess amount of Ag NPs can induce the phase change of NaYF$_4$ which will influence the upconversion efficiency; meanwhile too little amount of Ag NPs is different to 75 form hot spot.[26] Thus, the amount of noble metals is a critical element to improve Raman enhancement.

Taking into account the above reasons, in this work, we present a rational route to synthesize upconversion microcrystal (NaYF$_4$:Yb,Er), then NaYF$_4$:Yb,Er@SiO$_2$ were prepared by a

typical method. Subsequently, the deposition of high-density Ag nanoparticles onto the SiO_2 surface can be received by an in situ growth method. Our procedure for material fabrication is easily operated, low cost and scalable. The designed particles showed excellent Raman enhancement under NIR excitation with low power. Most importantly, the SiO_2 shell can prevent phase change of $NaYF_4$:Yb,Er because of the deposition of Ag NPs. Furthermore, the surface of SiO_2 exhibit highly biocompatible, easy surface modification, and easy control of interparticle interactions. This substrate exhibited an excellent sensitivity for methylamphetamine detection under near-infrared excitation. Lastly, NIR excitation has less harmful to the samples but greater sample penetration depths. The hybrid structures also provide a new direction for the synthesis of novel SERS substrates and promise many attractive potential applications for fast, simple, supersensitive and nondestructive SERS sesning.

Experimental Section

Chemicals and materials

Silver nitrate ($AgNO_3$), sodium citrate, para-aminothiophenol (PATP), NaF, $ErCl_3$, $YbCl_3·6H_2O$, $YCl_3·6H_2O$, ammonia, tetraethyl orthosilicate (TEOS), crystal violet (CV), and all of these were A.R. grade and obtained from Shanghai Reagent Co. without further purification, and their solutions were prepared with distilled water without further pH regulation. Methylamphetamine (MAMP) was gifted by Prof. Xie J. W. from the AMMS of the PLA, Beijing, China. The whole experiment was carried out in water system without any buffer, and all the experiments under room temperature (25℃).

Synthesis of upconversion materials

A hydrothermal method[27] was simply modified to synthesize UC microcrystals by using trisodium citrate as a capping agent. An aqueous solution of $YCl_3·6H_2O$, $YbCl_3·6H_2O$, and $ErCl_3$ (lanthanide ion molar ratio, Y/Yb/Tm= Y/Yb/Er = 88:10:2) was mixed with an aqueous solution of 1% trisodium citrate under vigorous stirring, producing a white complex. Then 1.2 mol/L NaF aqueous solution (25 mL) was added into the complex solution, which was stirred for 1 h. The newly-formed complex precursor solution was then transferred into a 60 ml autoclave and heated at 180℃ for 3 h. The $NaYF_4$:Yb,Er microcrystals were then separated via centrifugation and rinsed several times with ultrapure water.

Preparation of SiO_2 decorated $NaYF_4$:Yb,Er (UC@SiO_2 for short)

A typical procedure for coating SiO_2 onto UC microcrystals has been described as follows:[28] 40 mg UC microcrystals were dispersed in 60 mL mix solution (containing 50 mL ethanol and 10 mL ultrapure water) by sonication. Then 10 mL 28% ammonia and TEOS were added sequentially into the mixture. The different amounts of TEOS were added to obtain different thickness of silica shell. The mixture was then stirred for 2 h. The obtained products were centrifugally precipitated, and rinsed several times with ultrapure water, and then vacuum dried at 60℃ for 6 h.

Preparation of Ag nanoparticles decorated UC@SiO_2 (UC@SiO_2/Ag for short)

The decorating of Ag nanoparticles onto the UC@SiO_2 was performed by the use of trisodium citrate as both the coupling agent and the reductant. The dried UC@SiO_2 powders were dispersed in ultrapure water, and 0.1mol/L $AgNO_3$ (0.25 mL) was added into the solution, and then the mixture solution was stirred and heated to 100℃. Then 1% trisodium citrate (1 mL) was added into the boiling solution, keep the temperature of the mixed solution for 1 hour. The obtained products were centrifugally precipitated, and rinsed several times with ultrapure water.

Synthesis of SiO_2 spheres

Silica spheres were prepared by using a typical method.[29] A solution of 30 mL of ammonia and 4 mL of tetraethoxysilane (TES) were added to 200 mL of dry ethanol under rapid stirring (>150rpm). The $NaYF_4$:Yb,Er microcrystals were then separated via centrifugation and rinsed several times with ultrapure water.

Preparation of Ag nanoparticles decorated SiO_2 (SiO_2@Ag for short)

The decorating of Ag nanoparticles onto the SiO_2 was performed by the use of trisodium citrate as both the coupling agent and the reductant. The dried SiO_2 powders were dispersed in ultrapure water, and 0.1mol/L $AgNO_3$ (0.25 mL) was added into the solution, and then the mixture solution was stirred and heated to 100℃. Then 1% trisodium citrate (1 mL) was added into the boiling solution, keep the temperature of the mixed solution for 1 hour. The obtained products were centrifugally precipitated, and rinsed several times with ultrapure water.

Synthesis of Ag NPs

Ag NPs were prepared by citrate reduction of $AgNO_3$.[30] 1 ml 0.1 M $AgNO_3$ was added into 99 ml ultra-pure water, and then the solution was brought to a vigorous boil with stirring in a round bottom flask fitted with a reflux condenser and heated to 100℃. 10g/L trisodium citrate (4 ml) was then added rapidly to the solution, keep the temperature of the mixed solution for 1 hour. The obtained products were centrifugally precipitated, and rinsed several times with ultrapure water.

Apparatus

The scanning electron microscopy (SEM) images were taken by a Sirion 200 field-emission scanning electron microscope. X-Ray scattering patterns were conducted by analyzing the powder samples on a Philips X-Pert Pro X-ray diffractometer (XRD) with Cu Ka radiation. Transmission electron microscopy (TEM) images were recorded by a JEOL 2010 high resolution transmission electron microscope, equipped with X-ray energy dispersive spectroscopy (EDS) capabilities, operated at an acceleration voltage of 200 kV. Upconversion luminescence spectra were recorded by a fluorescence spectrophotometer under the excitation of a 980 nm laser. Raman spectra were carried out on a LabRAM HR800 confocal microscope Raman system (Horiba Jobin Yvon) using an Ar ion laser operating at 785 nm. The laser power was approximately 1 mW. All of the spectra reported were the results of a single 1 s accumulation.

Results and Discussion

The UC cores can efficiently convert NIR excitation into visible light, we speculated that coupling the UC with noble metals is an attractive and promising strategy to solve the LSPR problem between photons incident and the nanoparticles. As shown in scheme 1 and Fig. S1, under the NIR excitation of 785 nm, the Yb^{3+} ions act as sensitizers and are the primary absorbers of the NIR excitation. Then Er^{3+} ions are excited from the $^4I_{15/2}$ ground state to the $^4I_{11/2}$ excited state via $Yb^{3+} \rightarrow Er^{3+}$ energy transfer. The luminescent states of Er^{3+} are excited by two consecutive $Yb^{3+} \rightarrow Er^{3+}$ energy transfer events, the first energy transfer is the $^4I_{15/2}$ ground state, and the second energy transfer is the long-lived intermediate excited state (i.e., $^4I_{13/2}$ or $^4I_{11/2}$). Then the Er^{3+} ion is excited to the $^4F_{7/2}$ state by a second $Yb^{3+} \rightarrow Er^{3+}$ energy transfer. After that, the Er^{3+} ion decays nonradiatively to the $^2H_{11/2}$, $^4S_{3/2}$ and $^4F_{9/2}$ levels, which gives the dominant green luminescence ($^2H_{11/2} \rightarrow {}^4I_{15/2}$, $^4S_{3/2} \rightarrow {}^4I_{15/2}$).[31-33] The red emission is obtained by the transition $^4F_{9/2} \rightarrow {}^4I_{15/2}$.[34, 35] After modification the UC by SiO_2 shell can prevent phase change of $NaYF_4$:Yb,Er and ensure the upconversion efficiency. In the presence of Ag NPs, the broad absorption of Ag can increased the power of the excitation by local field enhancement, resulting in the increase of excited Yb^{3+} ions, and more energy transfer from excited Yb^{3+} to Er^{3+}.[36] The highly enhanced local field density induced by the plasmon field enhancement effect will act on the SERS effects. In addition, the green emission bands at 520, 528 and 540 nm are attributed to $^2H_{11/2} \rightarrow {}^4I_{15/2}$ and $^4S_{3/2} \rightarrow {}^4I_{15/2}$ transitions for Er^{3+} ions, respectively. The green emission bands at 520, 528 and 540 nm can be treated as an excess laser effect on Ag surfaces. The plasmon resonance at the excitation lasers of green emissions becomes stronger, and consequently a higher sensitivity was obtained on Ag NPs of which the LSPR appears in the UV/visible spectral range.[37]
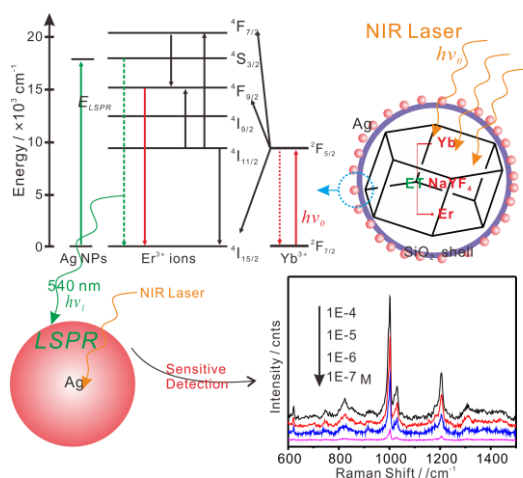
Scheme 1. Illustration of the relevant processes of energy transfer in UC@SiO$_2$@Ag particles and the local electric field, E$_{LSPR}$, enhanced by the LSPR of Ag NPs.

In the aspect of experiments, the hexagonal $NaYF_4$:Yb,Er microcrystals with the uniform size and shape were successfully synthesized by a simple hydrothermal method, their average side length was ~600 nm (Fig. 1A). To date, $NaYF_4$ has been widely recognized as one of the most efficient hosts for upconversion rare-earth (RE) ions sensitized by Yb^{3+}. To prevent phase change of $NaYF_4$:Yb,Er and ensure the upconversion efficiency, a uniform silica layer was coated on their surface by a typical method. The layer consists of amorphous SiO_2, and the thickness of silica shell can be adjusted by the different amounts of TEOS as shown in Fig.1B-D. The volumes of TEOS solution were set to 50, 25 and 15 µl to obtain silica thicknesses were 100, 50 and 7 nm, respectively. To ensure the incident light can be effective absorbed by UC cores, we selected the 7 nm silica thicknesses in the following experiments.
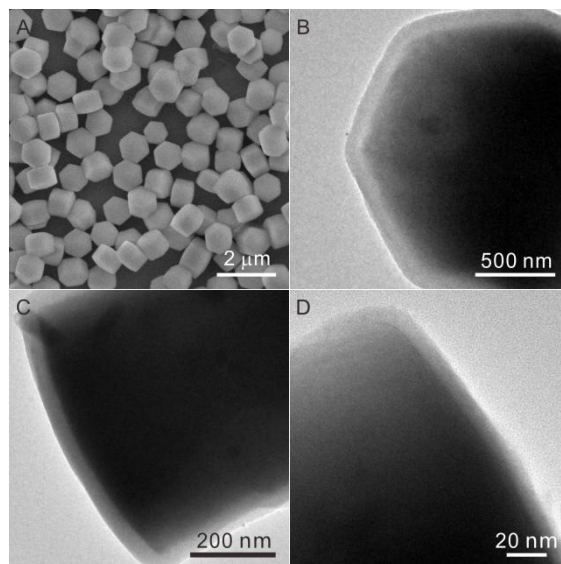

Fig. 1 SEM image of $NaYF_4$:Yb,Er NCs. (B-D) TEM images of UC@SiO$_2$ particles, different thickness of silica shell were 100 nm, 50 nm and 7 nm, respectively.
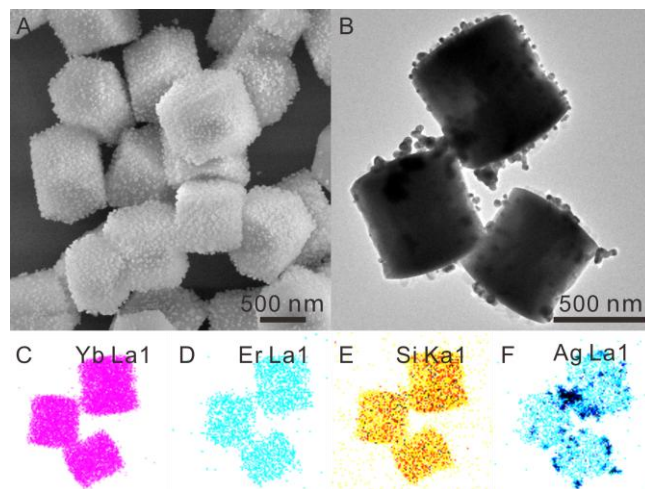

Fig. 2 (A-B) SEM and TEM images of UC@SiO$_2$@Ag particles (inset in B: the corresponding emission spectrum of UC@SiO$_2$@Ag). (C-F) EDX elemental mapping of a single particle of UC@SiO$_2$@Ag, including Yb La1, Er La1, Si Ka1 and Ag La1.

After coating UC microcrystals with SiO_2, a simple procedure was developed to decorate high-density Ag NPs on the surface of this composite microcrystal. As shown in Fig. 2A and B, the dense Ag NPs were successfully decorated on the surface of

NaYF$_4$:Yb,Er@SiO$_2$, and the main visible emission peaks of UC@SiO$_2$@Ag centered at 540 and 652 nm (inset in Fig. 2B). The HRTEM at high angle annular dark field (HAADF) evidenced that all elements of Yb, Er, Si, and Ag distributed throughout the entire particle (Fig. 2C-F). The elemental mapping profiles also provided exclusive evidence of the presence of the metals, their distribution pattern, and the progressive wrapping of the Ag decorated NaYF$_4$:Yb,Er@SiO$_2$. The extinction spectrum of NaYF$_4$:Yb,Er@SiO$_2$@Ag substrate was shown in Fig. S2. The extinction spectrum showed a broad absorption covered the visible light range. The red shift of the LSPR of Ag NPs may due to the formation of very big clusters and decrease the interparticle gaps when Ag NPs deposited on the NaYF$_4$:Yb,Er@SiO$_2$.

The XRD pattern of UC microcrystals (curve a in Fig. 3A) was in good agreement with the standard values of the hexagonal-phase NaFY$_4$ crystals (JCPDS files No.28-1192). Hexagonal NaFY$_4$ is a more efficient host for upconversion luminescence than cubic NaFY$_4$ and YF$_3$. The curve b in Fig. 3A was the XRD patterns of SiO$_2$-decorated UC microcrystals, due to the amorphous nature, no defined peak from the silica shell was observed except a small uplift on the baseline at the low angle region, which may be caused by the diffraction between irregular molecule layers of amorphous SiO$_2$.[38] The detail information of broad diffraction band locating between 20° and 30° comes from porous SiO$_2$ can be seen clearly in the Fig. S3.[26] The new peaks at 2θ = 38.0, 44.2, 64.4, and 77.3 in curve c in Fig. 3A were consistent with the face Ag (JCPDS files No.87-0720). Fig. 3B presented the PL spectra of UC microcrystals (green line), UC@SiO$_2$ (black line) and UC@SiO$_2$@Ag (red line) under the NIR excitation. The intensities of 520, 528, 540, and 652 nm peaks originated from UC microcrystals were 86000, 65000, 200000 and 62000 cnts, respectively. The very thin shell of SiO$_2$ has a little influence on the PL spectrum, and the intensities of 520, 528, 540, and 652 nm peaks originated from UC@SiO$_2$ were 60000, 45000, 175000, and 39000 cnts, respectively. It's worth noting that the coating of Ag on UC microcrystals results in remarkable enhancement of PL spectrum. The intensities of 520, 528, 540, and 652 nm peaks originated from UC@SiO$_2$@Ag were 81000, 65000, 230000, and 94000 cnts, respectively. We can deduce that the main reason is the existence of Ag. In the presence of noble metals NPs, such as Au and Ag NPs, the broad absorption of noble metals can increase the power of the excitation by local field enhancement, resulted in the increase of excited Yb^{3+} ions, and more energy was transferred from excited Yb^{3+} to Er^{3+}.[36]
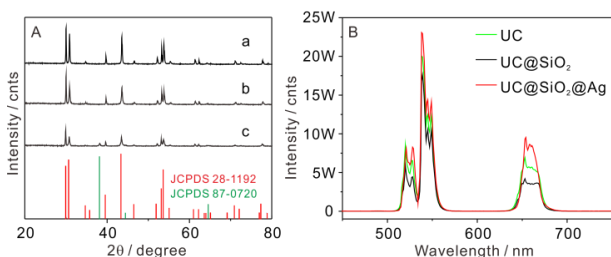

Fig.3 (A) XRD patterns of UC microcrystals (a) UC@SiO$_2$ (b) and UC@SiO$_2$@Ag (c) and standard XRD patterns of NaYF$_4$ (JCPDS 28-1192) and Ag (87-0702). (B) PL spectra of UC microcrystals (green line),

UC@SiO$_2$ (black line) and UC@SiO$_2$@Ag (red line) under the NIR excitation.

To verify the SERS capability of UC@SiO$_2$@Ag, a series of experiment were carried out by the use of 4-aminothiophenol (PATP), a widely-used SERS reporter, as the target molecule. The UC@SiO$_2$@Ag was first modified with 1 µM of PATP in ethanol for 5 min and then washed thoroughly by water. The PATP molecule was adsorbed on Ag surface as thiolate after S-H bond cleavage, and the covalent Ag–S interaction should be much stronger than other interactions,[16] and a dense single-molecular monolayer of PATP should be adsorbed on the Ag surface. Finally, 5 µL of the diluted suspension was dispersed on the surface of silicon wafers. And single-particles of UC@SiO$_2$@Ag was found under the optical microscopy and used for the SERS measurements.
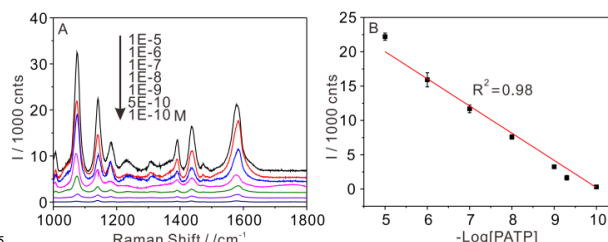

Fig. 4 (A) SERS spectra obtained from different concentrations of PATP using UC@ SiO$_2$@Ag, and (B) the linear correlation of Raman intensity at 1142 cm^{-1} with the logarithm of PATP concentrations.

To prove the sensitivity of UC@Ag substrate, SERS spectra of PATP were collected by varying its concentration from 10^{-5} to 10^{-10} M under 785 nm, as shown in Fig. 4A. Under the NIR excitation, Er^{3+} ion decays nonradiatively to the ^{2}H$_{11/2}$, ^{4}S$_{3/2}$ and ^{4}F$_{9/2}$ levels, which gives the dominant green luminescence (^{2}H$_{11/2}$ → ^{4}I$_{15/2}$, ^{4}S$_{3/2}$ → ^{4}I$_{15/2}$). When the green emission bands at 520, 528 and 540 nm effect on the on Ag surfaces, the highly plasmon resonance will be induced because the LSPR of Ag NPs appears in the visible spectral range, resulting in excellent SERS detection. The intensity of the strongest peak at 1142 cm^{-1} (Fig. 4B) was used for the quantitative evaluation of the detection level and exhibited a good linear relationship with the concentration ranging from 1.0×10^{-5} to 1.0×10^{-10} M (R^2 = 0.98). The limit of detection was determined to be 1.0×10^{-10} M from three standard deviations above the background.

As a reference, 5 µL of the 100-fold concentrated Ag sols dried in air on the surface of silicon wafer can form the multilayers of Ag NPs. The interparticle gap among Ag substrate was less than 5 nm (Fig. S5A) that can maximize the localized electric field and greatly amplify the Raman signals of target molecules. The UV-vis diffused reflectance absorption spectra of dry Ag substrate showed two peaks located at 411 and 538 nm (Fig. S5B). The red shift of the LSPR of Ag may due to the formation of very big clusters and decrease the interparticle gaps when the substrate is dried. The intensity of the 1434cm^{-1} peak of PATP adsorbed on UC@SiO$_2$@Ag is about 5.3 times larger than that obtained on Ag substrate, as shown in Fig. S5C-D. The shape, LSPR and size of the Ag NPs decorated on NaYF$_4$:Yb,Er@SiO$_2$ were similar to that of the pure Ag NPs. More importantly, the interparticle gaps among the Ag NPs decorated on NaYF$_4$:Yb,Er were larger than that of Ag substrate and the density is lower than that of Ag

substrate, which will reduce the coupling of the Ag NPs. Therefore, it should be the presence of UC materials that contributed to the greatly improved SERS performance of UC@SiO₂@Ag.
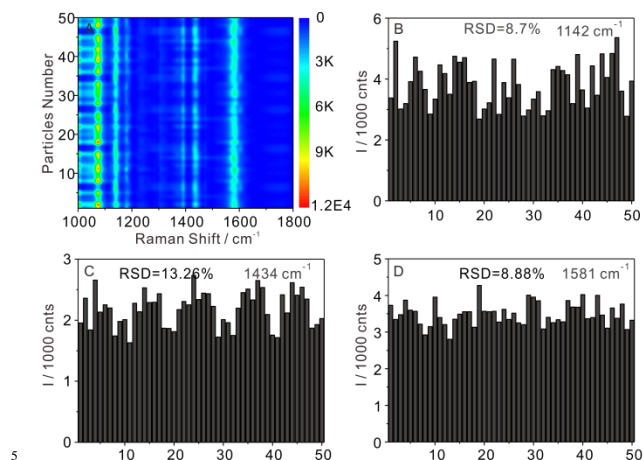

Fig. 5 (A) A series of SERS spectra of 10^{-6} M PATP molecules collected on 50 randomly selected particles of the UC@SiO₂@Ag and (B-D) the intensities at 1142, 1434 and 1581 cm⁻¹ of PATP.

The problem of reproducibility has always been a critical issue in SERS, which has hampered the progress of SERS technology. Therefore, uniformity and reproducibility of SERS substrates must be validated. Fig. 5A showed the SERS spectra of PATP collected on UC@SiO₂@Ag under 785 nm. The distinctive bands of PATP molecules can be observed at 1072, 1142, 1392, 1434 and 1581 cm⁻¹.[39] The intensity of the main vibration of PATP from 50 particles of SERS data was shown and indicating excellent reproducibility. To get a statistically result, the relative standard deviation (RSD) of the Raman intensity of the carbon skeleton stretching modes was calculated.[25] The RSD of the Raman vibrations at 1142, 1434 and 1581 cm⁻¹ were 8.7%, 13.26% and 8.88%, respectively (Fig. 5B-D), which clearly revealing the high reproducibility of the substrate.
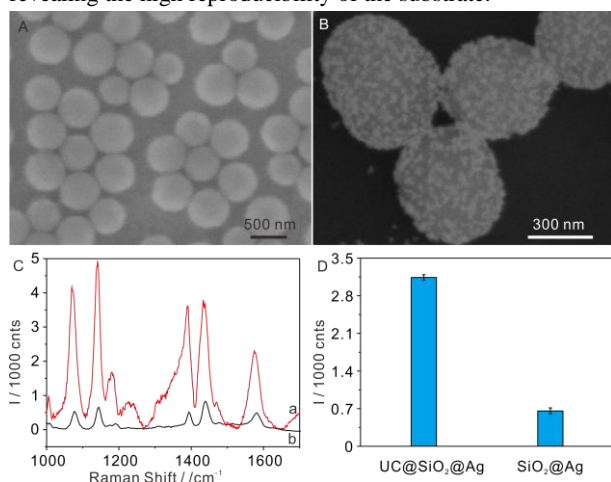

Fig 6 (A) SEM image of SiO₂, (B) SEM image of SiO₂@Ag. (C) The SERS spectra of 10^{-6}M PATP under 785 nm on (a) UC@SiO₂@Ag, (b) SiO₂@Ag; (D) The comparison of enhancement effects at 1434 cm⁻¹ of the two substrates.

The UV-Vis absorbance spectrum of dry Ag substrate showed two peaks located at 411 and 538 nm (Fig. S5B), while that of NaYF4:Yb,Er@SiO₂@Ag substrate showed a broad absorption covered the visible light range (Fig. S2). The UC@SiO₂@Ag nanoparticles have a larger extinction at 785 nm as compared with the Ag substrate. The red shift of LSPR may due to the formation of very big clusters and decrease the interparticle gaps when Ag NPs deposited on the NaYF4:Yb,Er@SiO₂. This will lead to a larger field enhancement (at 785 nm) and therefore larger SERS enhancement for the UC@SiO₂@Ag nanoparticles, as shown in Fig.S5C and Fig.S6A. However, the SERS enhancement upon excitation at 633 and 532 nm (Fig.S6C and S6D) is similar for both the UC@SiO₂@Ag nanoparticles and the Ag substrate. The LSPR effect should be a factor of the observed SERS enhancement.

To demonstrate the key role of UC cores in SERS performance under NIR excitation, we have done such an experiment by comparing the Raman signals attained from the Ag NPs decorated UC@SiO₂ microcrystals and AgNP decorated same size dielectric microcrystals without non-linear properties. We synthesized the spherical SiO₂ particles with the similar size. The SiO₂ are uniform, with the diameter of ∼600 nm (Fig. 6A), the Ag NPs had been successfully decorated on SiO₂ as shown in Fig. 6B. Fig. 6C showed the SERS spectra of PATP collected on UC@SiO₂@Ag (curve a) and SiO₂@Ag (curve b) under 785 nm. As shown in Fig. 6D, the intensity of the 1434cm⁻¹ peak is only about 650 cnts produced by the SiO₂@Ag. The corresponding SERS intensity of the 1434cm⁻¹ peak of PATP adsorbed on UC@SiO₂@Ag is about 3150 cnts, which is nearly 5 times larger than that obtained on SiO₂@Ag. The method, shape and size of the Ag NPs decorated on UC@SiO₂ were similar to that decorated on SiO₂. Therefore, it should be the presence of UC materials that contributed to the greatly improved SERS performance of UC@SiO₂@Ag.

To further verify the improved SERS performance of UC@SiO₂@Ag, a resonant dye molecule 'crystal violet', also a widely-used SERS reporter, was used to examine these differences (Fig. S6). Similarly, the UC@SiO₂@Ag has much better SERS performance than Ag substrate. The intensity of the 1172 cm⁻¹ peak of CV adsorbed on UC@SiO₂@Ag is about 6.7 times larger than that obtained on Ag substrate (Fig. S6B). As the longitudinal comparison of a same sample, another two different monochrome laser lines (532 nm and 633 nm) were employed to carry out SERS experiments. As shown in Fig S5C-D, the SERS intensity of CV adsorbed on UC@SiO₂@Ag is a little weaker than that obtained on Ag substrate. The probable reason is that UC cannot efficiently convert the lasers of 532 nm and 633 nm into visible light to improved SERS performance. Moreover, the interparticle gaps among the Ag NPs decorated on NaYF4:Yb,Er were larger than that of Ag substrate and the density is lower than that of Ag substrate (Fig.2A), which will reduce the coupling of the Ag NPs. Therefore, it should be the presence of UC materials that contributed to the greatly improved SERS performance of UC@SiO₂@Ag under NIR excitation.

The synthetic method, particle shape and size of the Ag NPs decorated SiO₂ (Fig. 6B) were similar to UC@SiO₂@Ag, which were further evidenced by their extinction spectra (Fig. S2 and S7). But the comparison between Fig.6D and Fig.S6B showed that the SERS intensity of the 1434cm⁻¹ peak of PATP adsorbed

on UC@SiO$_2$@Ag is nearly 5 times larger than that obtained on SiO$_2$@Ag, and that the corresponding peak intensity of SiO$_2$@Ag is slightly larger than that of Ag multilayer. Hence, the presence of UC materials contributed the major part of SERS enhancement of UC@SiO$_2$@Ag nanoparticles under NIR excitation. Hence, the main reason of dramatic SERS enhancement for UC@SiO$_2$@Ag nanoparticles under NIR excitation can be concluded that the presence of UC materials induced high local field density. Consequently, the Raman signals of molecules also become stronger with higher Raman cross-section and dipole moment induced by the high local field density.
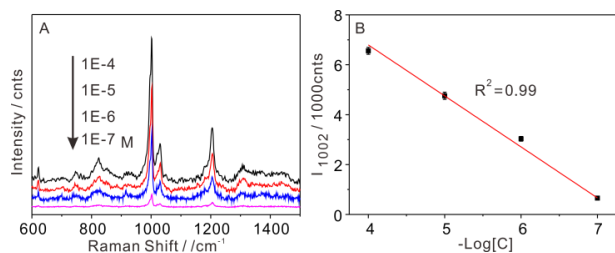

Fig. 7 (A) SERS spectra obtained from different concentrations of MAMP using UC@ SiO$_2$@Ag, and (B) the Raman intensity at 1002 cm^{-1} with the logarithm of MAMP concentrations.

The practical application is also an important issue in SERS detection, which has became one of the key points on the value evaluation of the substrate. Generally, the laser with longer wavelengths will have much deeper penetration depth and relatively smaller damage to the sample, e.g. 785 nm laser used in this work, which are suitable for practical application. To test the potential practical-detection power of the UC@SiO$_2$@Ag, we have used it to collect SERS spectra of MAMP, a particularly popular drug of abuse in the world.[40] Fig. 7A showed the SERS spectra of MAMP solution with different concentrations from 10^{-4} M to 10^{-7} M, deposited onto UC@SiO$_2$@Ag particles. The spectra were observed containing peaks at 1002, 1030 and 1206 cm^{-1}, all the peaks belong to methamphetamine Raman bands.[41] The intensity of the strongest peak at 1002 cm^{-1} (Fig. 7B) was used for the quantitative evaluation of the detection level and exhibited a good linear relationship with the concentration ranging from 1.0×10^{-4} to 1.0×10^{-7} M (R^2 = 0.99). The limit of detection was determined to be 1.0×10^{-7} M from three standard deviations above the background.

Conclusions

In closing, the uniform UC@SiO$_2$@Ag composite were prepared by a simple and efficient method, which is also incorporated into SERS-active substrates. The best thickness of silica shell can be easily obtained by adjusting the amounts of TEOS, which is the crucial elememt to balance the upconversion of UC and the hot spot formation by Ag NPs aggregation. The presence of UC materials provides more excitation lines and much stronger plasmon resonance under 785 nm. As prepared UC@SiO$_2$@Ag particles show several outstanding properties, such as excellent sensitivity, high-density Ag nanoparticles and high reproducibility under near–infrared excitation, which render them ideal candidates for various applications. Such UC@SiO$_2$@Ag is

an excellent sensitive probe for MAMP detection. This finding shed a new light on applications of UC-noble metal composites and also promises a novel direction for fabricating SERS-active nanostructures.

Notes and references

Institute of Intelligent Machines, Chinese Academy of Sciences, Hefei 230031, China.
Phone: +86-551-6559-2385. Fax: +86-551-6559-2420. E-mail: hlliu@iim.ac.cn, lbyang@iim.ac.cn.

† Electronic Supplementary Information (ESI) available: [Raman, XRD and EDX]. See DOI: 10.1039/b000000x/

1. H. L. Liu, Z. L. Yang, L. Y. Meng, Y. D. Sun, J. Wang, L. B. Yang, J. H. Liu and Z. Q. Tian, J. Am. Chem. Soc., 2014, 136, 5332-5341.
2. W. B. Caldwell, D. J. Campbell, K. M. Chen, B. R. Herr, C. A. Mirkin, A. Malik, M. K. Durbin, P. Dutta and K. G. Huang, J. Am. Chem. Soc., 1995, 117, 6071-6082.
3. J. F. Li, Y. F. Huang, Y. Ding, Z. L. Yang, S. B. Li, X. S. Zhou, F. R. Fan, W. Zhang, Z. Y. Zhou, D. Y. Wu, B. Ren, Z. L. Wang and Z. Q. Tian, Nature, 2010, 464, 392-395.
4. T. Wang, F. Hu, E. Ikhile, F. Liao, Y. Q. Li and M. W. Shao, J. Mater. Chem. C, 2015, 3, 559-563.
5. M. T. Sun, Z. L. Zhang, H. R. Zheng and H. X. Xu, Sci. Rep.-Uk, 2012, 2.
6. W. Xie, C. Herrmann, K. Kompe, M. Haase and S. Schlucker, J. Am. Chem. Soc., 2011, 133, 19302-19305.
7. Y. F. Huang, H. P. Zhu, G. K. Liu, D. Y. Wu, B. Ren and Z. Q. Tian, J. Am. Chem. Soc., 2010, 132, 9244-9246.
8. J. A. Creighton, C. G. Blatchford and M. G. Albrecht, J. Chem. Soc. Farad T 2, 1979, 75, 790-798.
9. A. J. Haes, C. L. Haynes, A. D. McFarland, G. C. Schatz, R. R. Van Duyne and S. L. Zou, Mrs. Bull., 2005, 30, 368-375.
10. A. D. McFarland, M. A. Young, J. A. Dieringer and R. P. Van Duyne, J. Phys. Chem. B, 2005, 109, 11279-11285.
11. J. Zhao, J. A. Dieringer, X. Y. Zhang, G. C. Schatz and R. P. Van Duyne, J. Phys. Chem. C, 2008, 112, 19302-19310.
12. J. A. Dieringer, K. L. Wustholz, D. J. Masiello, J. P. Camden, S. L. Kleinman, G. C. Schatz and R. P. Van Duyne, J. Am. Chem. Soc., 2009, 131, 849-854.
13. M. Grabiec, A. Wolak, O. Veron, J. P. Blondeau, N. Pellerin, M. Allix, S. Pellerin and K. Dzierzega, Plasmonics, 2012, 7, 279-286.
14. G. K. Liu, J. Hu, P. C. Zheng, G. L. Shen, J. H. Jiang, R. Q. Yu, Y. Cui and B. Ren, J. Phys. Chem. C, 2008, 112, 6499-6508.
15. S. Jabeen, T. J. Dines, R. Withnall, S. A. Leharne and B. Z. Chowdhry, Phys. Chem. Chem. Phys., 2009, 11, 7476-7483.
16. H. L. Liu, Y. D. Sun, Z. Jin, L. B. Yang and J. H. Liu, Chem. Sci., 2013, 4, 3490-3496.
17. B. Crisan, O. Soritau, M. Baciut, R. Campian, L. Crisan and G. Baciut, Particul. Sci. Technol., 2013, 31, 168-173.
18. A. Lee, G. F. S. Andrade, A. Ahmed, M. L. Souza, N. Coombs, E. Tumarkin, K. Liu, R. Gordon, A. G. Brolo and E. Kumacheva, J. Am. Chem. Soc., 2011, 133, 7563-7570.
19. H. C. Jeon, C. J. Heo, S. Y. Lee and S. M. Yang, Adv. Funct. Mater., 2012, 22, 4268-4274.
20. W. Feng, L. D. Sun and C. H. Yan, Chem. Commun., 2009, 4393-4395.
21. F. Wang, Y. Han, C. S. Lim, Y. H. Lu, J. Wang, J. Xu, H. Y. Chen, C. Zhang, M. H. Hong and X. G. Liu, Nature, 2010, 463, 1061-1065.

Analyst Accepted Manuscript

22. Y. Wu, X. Shen, S. X. Dai, Y. S. Xu, F. F. Chen, C. G. Lin, T. F. Xu and Q. H. Nie, J. Phys. Chem. C, 2011, 115, 25040-25045.
23. J. C. Goldschmidt, S. Fischer, H. Steinkemper, F. Hallermann, G. von Plessen, K. W. Kramer, D. Biner and M. Hermle, Ieee J. Photovolt., 2012, 2, 134-140.
24. P. Zhao, Y. H. Zhu, X. L. Yang, K. C. Fan, J. H. Shen and C. Z. Li, Rsc Adv., 2012, 2, 10592-10597.
25. Y. M. Ma, H. L. Liu, Z. Z. Han, L. B. Yang, B. Sun and J. H. Liu, Analyst, 2014, 139, 5983-5988.
26. L. N. Liu, C. J. Tang, Y. S. Zhang, C. H. Zang, D. M. Zhang, H. Y. Xiao, R. F. Qin and Z. G. Bao, J. Alloy. Compd., 2014, 591, 320-325.
27. Y. J. Sun, Y. Chen, L. J. Tian, Y. Yu, X. G. Kong, J. W. Zhao and H. Zhang, Nanotechnology, 2007, 18.
28. Y. L. Ding, X. D. Zhang, H. B. Gao, S. Z. Xu, C. C. Wei and Y. Zhao, J. Lumin., 2014, 147, 72-76.
29. D. L. Shao, H. T. Sun, M. P. Yu, J. Lian and S. Sawyer, Nano Lett, 2012, 12, 5840-5844.
30. P. C. Lee and D. Meisel, J Phys Chem-Us, 1982, 86, 3391-3395.
31. S. Schietinger, T. Aichele, H. Q. Wang, T. Nann and O. Benson, Nano Lett., 2010, 10, 134-138.
32. G. S. Qin, W. P. Qin, C. F. Wu, S. H. Huang, J. S. Zhang, S. Z. Lu, D. Zhao and H. Q. Liu, J. Appl. Phys., 2003, 93, 4328-4330.
33. H. R. Zheng, D. L. Gao, Z. X. Fu, E. K. Wang, Y. Lei, Y. Tuan and M. Cui, J. Lumin., 2011, 131, 423-428.
34. J. H. Wu, J. L. Wang, J. M. Lin, Z. Lan, Q. W. Tang, M. L. Huang, Y. F. Huang, L. Q. Fan, Q. B. Li and Z. Y. Tang, Adv. Energy Mater., 2012, 2, 78-81.
35. H. P. Paudel, L. L. Zhong, K. Bayat, M. F. Baroughi, S. Smith, C. K. Lin, C. Y. Jiang, M. T. Berry and P. S. May, J. Phys. Chem. C, 2011, 115, 19028-19036.
36. N. Liu, W. P. Qin, G. S. Qin, T. Jiang and D. Zhao, Chem. Commun., 2011, 47, 7671-7673.
37. J. D. Driskell, R. J. Lipert and M. D. Porter, J. Phys. Chem. B, 2006, 110, 17444-17451.
38. Z. Q. Li, L. M. Wang, Z. Y. Wang, X. H. Liu and Y. J. Xiong, J. Phys. Chem. C, 2011, 115, 3291-3296.
39. X. G. Hu, T. Wang, L. Wang and S. J. Dong, J. Phys. Chem. C, 2007, 111, 6962-6969.
40. N. Stojanovska, S. L. Fu, M. Tahtouh, T. Kelly, A. Beavis and K. P. Kirkbride, Forensic Sci. Int., 2013, 224, 8-26.
41. C. Andreou, M. R. Hoonejani, M. R. Barmi, M. Moskovits and C. D. Meinhart, ACS NANO, 2013, 7, 7157-7164.